Shortwave Infrared Spectroradiometer for Atmospheric Transmittance Measurements

M. SICARD,* K. J. THOME, B. G. CROWTHER, AND M. W. SMITH+

Remote Sensing Group, Optical Sciences Center, The University of Arizona, Tucson, Arizona

(Manuscript received 23 January 1997, in final form 22 May 1997)

ABSTRACT

The use of a shortwave infrared (SWIR) spectroradiometer as a solar radiometer is presented. The radiometer collects 1024 channels of data over the spectral range of 1.1–2.5 μm. The system was tested by applying the Langley method to data collected at a high altitude site on two consecutive days. Data processed for the 1.15–1.32-μm and 1.47–1.75-μm spectral intervals show temporal results similar to those obtained with a well-understood, visible, and near-infrared radiometer having 10 channels in the 0.38–1.03-μm spectral range. A modified Langley method was used for spectral regions where strong water vapor absorption invalidates the Langley method. It is estimated that the exoatmospheric intercept of the spectroradiometer was determined to better than 4% in nonabsorption regions between 1.15 and 1.75 μm and to better than 5% for a large portion of the 1.38-μm absorption band. These results, in addition to the agreement between the shortwave, and the visible and near-infrared radiometers, imply that the SWIR system operates well as a solar radiometer. The spectral optical depths from one day were used to determine a power-law aerosol size distribution using data from both the visible and near-infrared, and the shortwave infrared. The exponent derived for this power law differed from that obtained by using only the visible and near-infrared by 6%. Aerosol optical depths in the shortwave infrared derived from the visible and near-infrared results differed from the measured values by 0.005 at an optical depth of 0.016 and wavelength of 1.66 μm.

1. Introduction

Currently, solar radiometer measurements made by the Remote Sensing Group of the Optical Sciences Center at The University of Arizona cover the 0.38–1.03-μm spectral range. These measurements are typically used in the reflectance- and radiance-based calibration methods for in-flight calibration of satellite and airborne remote sensors (Slater et al. 1987). These methods are planned for the in-flight radiometric calibration of the moderate resolution imaging spectroradiometer (MODIS) and the advanced spaceborne thermal emission and reflection radiometer (ASTER) scheduled for a mid-1998 launch on NASA's Mission to Planet Earth, Earth Observing System AM-1 platform (Neeck et al. 1995). Both MODIS and ASTER have multiple bands in the shortwave infrared (SWIR) portion of the spectrum from 1.1 to 2.5 μm (Platnick et al. 1994; Fujisada 1995). Thus, it is important to extend our solar radiometer capabilities into the SWIR both to better quantify the atmospheric transmittance, and hence optical depths, and to better retrieve the number of larger aerosol particles. This will be especially useful for our future vicarious calibrations by allowing us to directly measure the atmospheric optical depths in the bands of the sensors we are calibrating, such as ASTER and MODIS.

Currently, we use data in the visible and near infrared (VNIR) part of the spectrum in an inversion scheme to retrieve a power-law exponent, or Junge parameter, to describe the aerosol size distribution (Biggar et al. 1990). The Junge parameter is used to derive the aerosol optical thickness in the bands of the sensor we are calibrating. The aerosol size distribution and aerosol optical thickness are large sources of uncertainties in vicarious calibration (Biggar et al. 1994). The fact that the solar radiometer we are studying in this work is hyperspectral means we will be able to determine directly the optical depths in the sensor bandpasses, rather than deriving them from the retrieved size distribution.

The purpose of this work is twofold. The first is to evaluate an SWIR spectroradiometer designed for surface reflectance retrieval for use as a solar radiometer. Second, we evaluate the effect of the retrieved SWIR optical depths on our retrieval of aerosol size distribution. The paper begins with a brief description of the instrument. Retrieved exoatmospheric signals using the Langley method are presented, followed by a discussion of the retrieved optical depth and atmospheric transmittance using these exoatmospheric signals. The re-

* Current affiliation: CIMEL Electronique, Paris, France.
+ Current affiliation: National Center for Atmospheric Research, Boulder, Colorado.

Corresponding author address: Michael Sicard, CIMEL Electronique, 5, Cite de Phalsbourg, 75011 Paris, France.
E-mail: m-sicard@worldnet.fr

trieved optical depths are compared to those from a well-understood solar radiometer operating in the VNIR portion of the spectrum. We then compare aerosol size distribution results from VNIR-only data to those derived from both VNIR and SWIR data. Included in this discussion are the effects of measurement uncertainties in the optical depths on the size distribution retrieval.

2. Instrument and data description

The spectroradiometer used in this work was originally built by the Remote Sensing Group for measuring surface reflectance (Smith 1992, 1994). The 1024 bands of the instrument cover the spectral range from 1.05 to 2.45 μm with a full-width at half-maximum bandwidth that can be selected from 0.005 to more than 0.100 μm. In the current work, the spectral resolution was selected to be 0.014 μm as suggested by the manufacturer when using the instrument with our heavy metal fluoride glass fiber-optic bundle. The minimum time to acquire a single spectrum is 1 s. For a 298-K background temperature, and a Lambertian surface of 100% reflectance illuminated by the sun at normal incidence with no atmospheric attenuation, the signal-to-noise ratio (SNR) is nearly 100 at a wavelength of 2.2 μm. For these same conditions, the SNR at 1.25 μm is nearly 900. Direct viewing of the sun gives a better SNR; however, saturation of the system at shorter wavelengths necessitates that we use a neutral density filter to retrieve usable data. Thus, the SNR values for the system used as a solar radiometer are similar to the values obtained when the system is used for reflectance data collection.

A flexible fiber-optic bundle couples the optics that define the field of view to the entrance slit of the spectroradiometer. A nonscanning, concave, holographic diffraction grating with flat focal field disperses and focuses the incoming radiation onto a linear-array detector with 1024 elements. The platinum-silicide detector array is liquid nitrogen cooled, and two absorption filters help determine the upper and lower wavelength limits of the system response. One of these filters is a silicon filter with transmittance less than 3% for wavelengths shorter than 1.05 μm. A cooled PK-50 filter with transmittance less than 3% for wavelengths longer than 3.1 μm reduces diffractive order effects. The diffraction grating housing is the main source of thermal background radiation and is thermally stabilized at 25°C, independent of ambient temperature, by two thermoelectric heat pumps.

The instrument was originally designed to be carried as a backpack unit. The original size of the system, excluding the collection optics, was about 48 cm $\times$ 38 cm $\times$ 23 cm with a total weight of about 18 kg. The system has since been modified to improve the SNR by cooling the diffraction grating housing. This increased the weight, size, and power requirements and reduced the portability.

The data are recorded in ASCII format by a portable computer with a built-in analog-to-digital converter. The memory size of this data logging computer allows 15 scans before data must be transferred to another computer. The system was designed with an 8° field of view. This is large enough that forward scattering effects from aerosols must be considered, and this effect is considered later in the paper.

To operate the system as a solar radiometer, the spectroradiometer is attached to a V block mounted to a tripod and is pointed using a pinhole pointing device on the V block. As mentioned previously, a neutral density filter is placed in front of the entrance aperture to reduce signal levels to below saturation. Unfortunately, this filter reduces the signal in the 2.0–2.5-μm range to a signal that is lower than desired. Since it is not feasible to switch filters during the data collection, this work concentrates on the 1.0–2.0-μm range.

The data presented in this paper were collected on Mount Lemmon at The University of Arizona's Steward Observatory, which is about 2800 m above sea level. The latitude is 32.44°N and the longitude is 110.79°W. The high altitude minimizes the effects of aerosol contamination and water vapor on optical depth measurements, thus improving the accuracy of the predicted signal at the top of the atmosphere. Two days worth of data were collected, comprising four total datasets of two sunrise and two sunset events. Forty-five data points were collected for each of the four datasets. Data were collected at 5-min intervals for a duration of 4 hours for each dataset.

3. The Langley method and intercept determination

The above datasets were processed using the Langley method that assumes Beer's law is valid and that attenuation by the atmosphere along the solar path varies linearly with the pathlength, then

$$\mathrm{DC}(\lambda) = \mathrm{DC}_0(\lambda) \times e^{-m\delta(\lambda)}, \quad (1)$$

where $\mathrm{DC}(\lambda)$ is the digital count output of the system at wavelength λ, $\mathrm{DC}_0(\lambda)$ is the exoatmospheric signal or DC intercept at wavelength λ, $\delta(\lambda)$ is the total vertical optical thickness at this wavelength, and m is the air mass computed from Kasten's model (Kasten and Young 1989). Strictly speaking, Beer's law only applies to the monochromatic case. In this work we are dealing with bandpasses that are on the order of 0.014 μm. While not monochromatic, the instrument responsivity and optical thicknesses due to molecular and aerosol extinction are smooth enough that band integration of the optical thicknesses and response is not necessary. This is not true for cases where there is strong gaseous absorption.

Taking the natural logarithm of both sides gives

$$\ln[\mathrm{DC}(\lambda)] = \ln[\mathrm{DC}_0(\lambda)] - m\delta(\lambda), \quad (2)$$

and it can be seen that $\ln[\mathrm{DC}(\lambda)]$ depends linearly on the optical thickness. To use the Langley method, a set

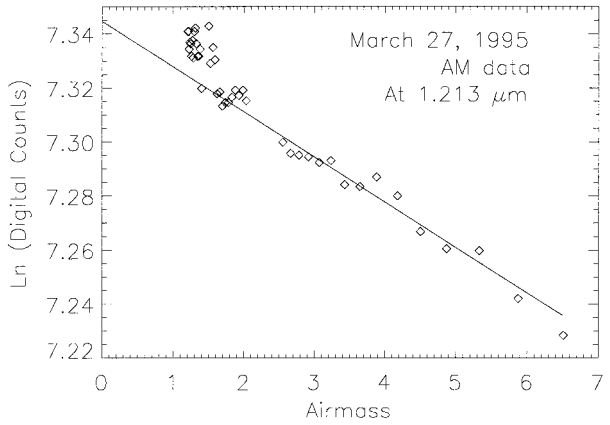

FIG. 1. Langley plot: logarithm of digital counts (DCs) vs air mass at the wavelength 1.213 μm from data of the morning of 27 March 1995. The straight line is the least squares best fit for the restricted airmass range from 2 to 6.5.

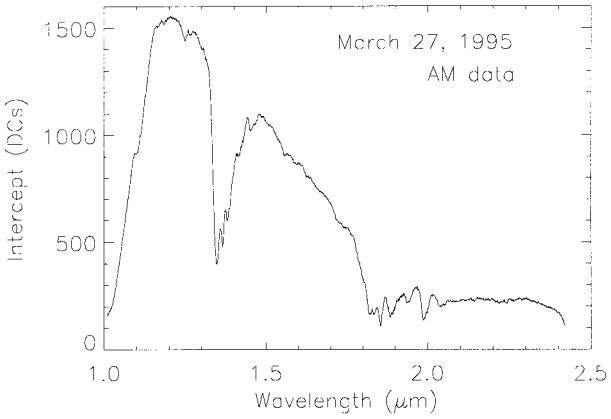

FIG. 2. Intercept vs wavelength from the data of the morning of 27 March 1995 for the restricted airmass range from 2 to 6.5.

of digital counts are recorded for a range of airmass values. By assuming the vertical optical depth is constant as a function of time, a straight-line fit to the ln(DC)s as a function of air mass will give the vertical optical depth, as well as the DC intercept.

An example of a Langley plot, graph of ln(DC) versus air mass from data collected on the morning of 27 March collected on Mount Lemmon with the SWIR spectroradiometer is shown in Fig. 1. These data are for a center wavelength of 1.213 μm and correspond to the largest DCs reported by the system. The gap in these data is due to the time needed to remove the data files from the data logging computer. The straight line shown in the figure shows the least squares fit to the data in the airmass range from 2.0 to 6.5. This restricted interval was selected because atmospheric effects later in the day invalidated the assumption of constant optical thickness. These atmospheric effects included strong winds, which began about midmorning and increased the aerosol loading, and convective activity due to solar heating of the ground that became more dominant during the later morning.

By applying the Langley method to all bands of the radiometer, we determined the intercept as a function of wavelength. Figure 2 shows the retrieved intercept as a function of wavelength for the results shown in Fig. 1. The sharp drops in the intercept around 1.38 and 1.80 μm are due to water vapor absorption. These lower intercepts occur because attenuation due to water vapor is not linear with absorber amount, invalidating the Langley method.

As described earlier, a total of four Langley datasets were collected during the two days on Mount Lemmon. We processed all four datasets in a similar fashion and computed the average intercept from the first three datasets. The fourth day is not included in the average because of the large uncertainties in the results due to atmospheric variability. The average intercepts and standard deviation of this average are shown in Fig. 3. From the figure it can be seen that the percent standard deviation is relatively constant in the 1.1–1.3-μm and 1.5–1.7-μm spectral ranges at about 2.5%–4.0%. The low SNR for wavelengths greater than 2.0 μm due to lower solar signal and poorer detector response is also apparent in the graph.

We can use Fig. 3 to draw several conclusions about the characteristics of the SWIR radiometer. The shape of the curve in the 1.0–1.3-μm spectral range shows the rise in detector response. It is offset in the 1.3–1.8-μm spectral range by the decreasing solar output. In the 1.8–2.5-μm spectral range, the signal is too low to be meaningful due to water vapor absorption in the 1.8–2.1-μm region and the lower solar irradiance and decreasing system response in the 2.1–2.5-μm region.

In addition to computing intercepts for the SWIR

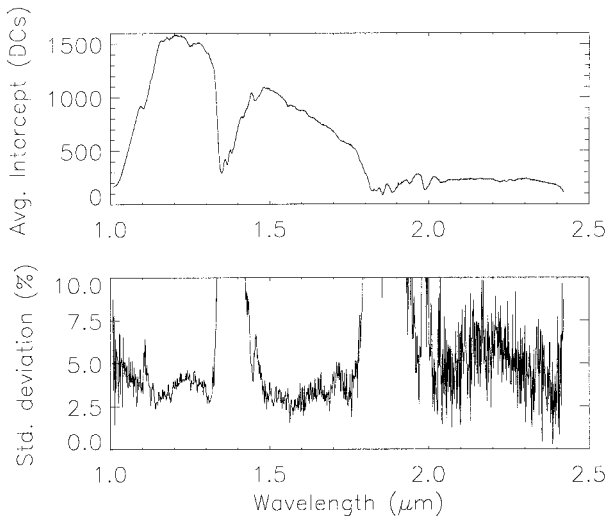

FIG. 3. Average intercept and standard deviation vs wavelength from data of the morning and afternoon of 27 March and morning of 28 March 1995. Intercepts were retrieved for airmass ranges from 2 to 6.5, 3 to 6.5, and 2.5 to 6, respectively.

TABLE 1. Repeatability results obtained for two wavelengths not affected by water vapor absorption of the SWIR instrument: 1.213 and 1.503 μm. DC_0 is the intercept and δ the optical depth. The average intercept and the percentage standard deviation are calculated only with the first three datasets. A comparison is also made with the bands 0.873 and 1.030 μm from the VNIR instrument.

	SWIR spectroradiometer				10-channel VNIR			
	1.213 μm		1.503 μm		0.873 μm		1.030 μm	
	DC_0	δ	DC_0	δ	DC_0	δ	DC_0	δ
03/27 am	1547.8	0.0167	1052.4	0.0159	1338.5	0.0285	903.49	0.0202
03/27 pm	1516	0.0242	1027	0.0215	1367.6	0.0470	917.82	0.0355
03/28 am	1635.2	0.032	1102.6	0.028	1359.9	0.0534	922.27	0.0426
03/28 pm	1513.5	0.0244	1048.2	0.0292	1372.9	0.0429	901.40	0.0336
Average DC_0	1566.3	—	1060.7	—	1359.7	—	911.25	—
% Std. dev.	3.9	—	3.6	—	1.1	—	1.1	—

spectroradiometer, we also computed intercepts for a 10-channel radiometer that covers the spectral range of 0.38–1.03 μm. This instrument was constructed by the Atmospheric Remote Sensing Laboratory of The University of Arizona Electrical and Computer Engineering Department. It has been used by the Remote Sensing Group as the primary solar radiometer for our vicarious calibration work for over 6 years and is believed to be well understood (Gellman et al. 1991). The instrument has 10 spectral bands with bandpasses of about 0.010 μm that are selected by manually turning a filter wheel. The radiometer is also manually aligned to the sun while data are logged to a computer.

Table 1 shows the retrieved intercept and average optical depth obtained from the Langley method for each of the four datasets for the four representative bands. The average intercept and standard deviation of this average for the first three datasets are also shown. The identical airmass ranges from Fig. 3 were used to generate these results. However, the fits do not include an identical number of points nor do the individual points match in time. The SWIR instrument records data essentially simultaneously in all bands, whereas data are recorded sequentially with the VNIR instrument. These differences could explain most of the disagreements between the two sets of data. The table shows that the intercepts from the SWIR instrument follow the same trend from one dataset to the next for all bands shown. This is not true of the VNIR data where the trend in the 0.873-μm band differs from the SWIR results, whereas the 1.03-μm band follows the same behavior except between the morning and afternoon of the first day. Observed optical depths of all four bands are lower in the morning when aerosol loading is expected to be smaller and increase in the afternoon when convection typically increases the amount of aerosols. The standard deviation of the SWIR radiometer is about three times larger than the one from the VNIR instrument but stays relatively small: 3.9% at 1.213 μm and 3.6% at 1.503 μm.

4. Instantaneous optical depth determination

The intercepts determined from the Langley method were used to compute the atmospheric optical depths as a function of time. Rearranging (2), the optical depth can be expressed as

$$\delta(\lambda) = \frac{\ln[DC_0(\lambda)] - \ln[DC(\lambda)]}{m}. \quad (3)$$

Figures 4a and 4b show optical depth as a function of wavelength for data collected during the morning of 27 March at an air mass of 4.50 and 1.21 using the average intercepts obtained from the method described in the previous section.

The effects of absorption are clear in both Figs. 4a and 4b. The large spikes around 1.38 and 1.80 μm correspond to the water vapor absorption mentioned earlier. Note these optical depths are not accurate because the strong absorption invalidates the Langley method. However, even with the incorrect intercepts, the effects due to absorption are quite evident. The small peaks in the optical depths at 1.13 and 1.27 μm are due to water vapor and carbon dioxide absorption, respectively. These features may be weak enough that the Langley method is still accurate, as suggested by Figs. 2 and 3 not showing significant departures in these spectral ranges.

The data shown in Fig. 4b are clearly noisier than those in Fig. 4a, but the spectral ranges 1.15–1.3 μm and 1.5–1.75 μm still give reasonably good results. One possible source of this noise is warming of the diffraction grating housing that was not adequately corrected for in the data collection. Clearly, also from Fig. 4b, the intercepts for many of the bands are incorrect since the optical thickness should not be less than zero. This is especially evident for wavelengths greater than 2.0 μm where the SNR is low. This effect also points to improper dark signal correction. These ''noisy'' optical depths were improved by averaging the raw data from several bands to improve the SNR and recomputing the intercepts. The resulting optical depths for an air mass of 1.21 are shown in Fig. 5. Note the disappearance of the negative optical depths (except for two points).

Figure 6 shows the retrieved optical depth as a function of time for data from both the VNIR and SWIR radiometers. To make visual comparison easier, data from the 0.87-μm channel of the VNIR radiometer are scaled and overlaid on the 1.213- and 1.503-μm chan-

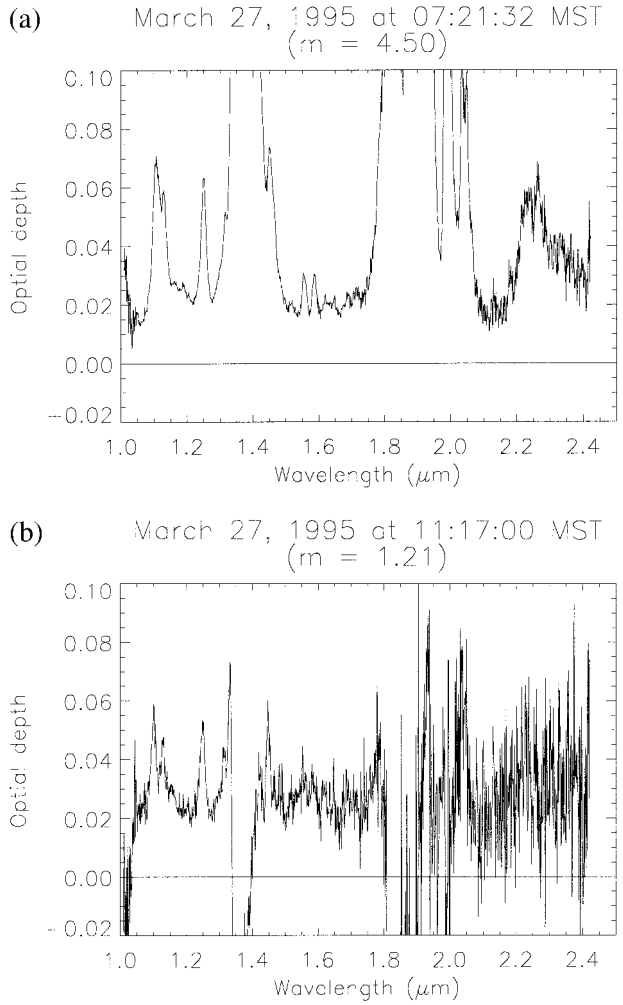

FIG. 4. (a) Optical depth vs wavelength from data of 27 March 1995 for an air mass of 4.50 using the average intercepts. (b) Optical depth vs wavelength from data of 27 March 1995 for an air mass of 1.21 using the average intercepts.

nels of the SWIR radiometer. Even though the wavelengths of the two systems are separated by nearly 0.34 μm and 0.63 μm, the temporal variability of the data should be similar. Figure 6 shows very good temporal agreement between the two instruments up until about 0800 LT. At this time, the SWIR data become more variable than the VNIR results, which remain fairly constant. This variability is more evidence of increasing noise problems later in the morning.

5. Modified Langley method

As mentioned previously, strong water vapor absorption invalidates the use of the Langley method because the attenuation is not linear with pathlength. This problem is avoided by using a modified Langley approach where the fit is no longer made to air mass, but rather (air mass)$^{1/2}$ (Thome et al. 1994). To test the feasibility

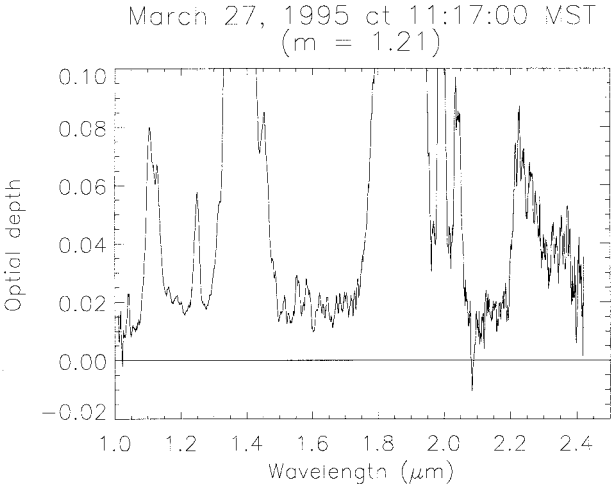

FIG. 5. Optical depth vs wavelength using the average intercepts of 27 March 1995 and a four-band spectral average at an air mass of 1.21.

of this approach, we applied the modified Langley method to the bands of the SWIR spectroradiometer affected by water vapor. The data used for the modified Langley analysis were corrected for aerosol and molecular scattering effects. Molecular optical depths were determined from the surface pressure. The aerosol optical depths in nonabsorption portions of the spectrum were determined as the difference between the retrieved total optical depth and the molecular optical depth. For bands with absorption, the aerosol optical depth is determined by assuming a power-law relationship and aerosol optical depths for low-absorption bands that bracket the band affected by absorption. Figure 7 shows a modified Langley plot for the morning of 27 March for 1.381 μm, where water vapor absorption is strong. The straight line

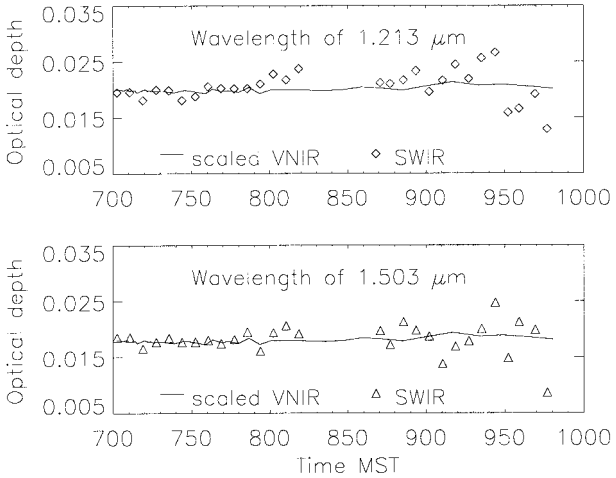

FIG. 6. Optical depth vs air mass at the wavelengths 1.213 and 1.503 μm from the SWIR instrument and scaled optical depth at the wavelength 0.873 μm from the VNIR instrument from data of the morning of 27 March 1995.

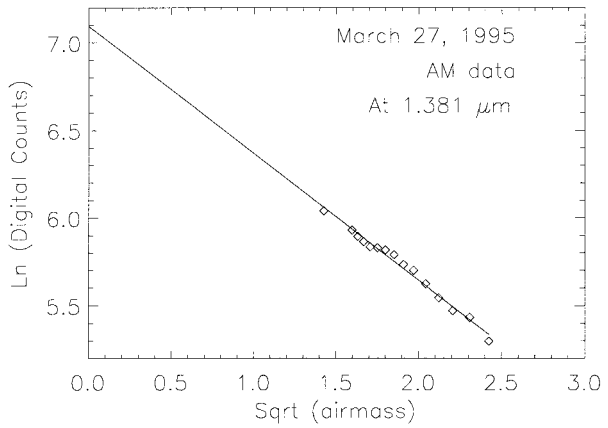

FIG. 7. Modified Langley plot: logarithm of digital counts (DCs) vs square root of air mass at the wavelength 1.381 μm from data of the morning of 27 March 1995 for the points where the air mass ranges between 2 and 6.5. The effect of aerosols on the total optical depth was removed by dividing the DCs by the aerosol transmittance at every air mass.

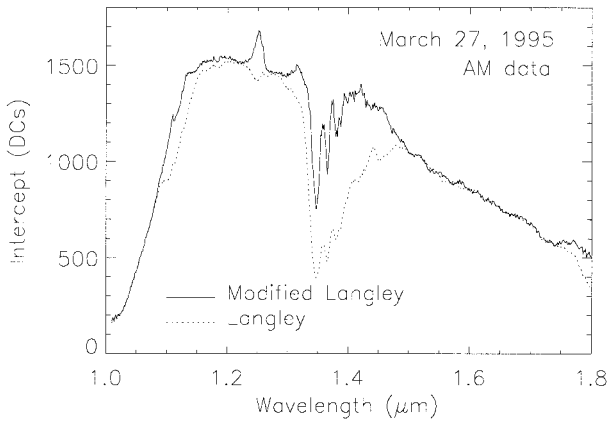

FIG. 8. Intercept from the Langley and the modified Langley methods vs wavelength from the data of the morning of 27 March 1995 for the restricted airmass range from 2 to 6.5.

in the figure shows the least squares fit to the data shown. Figure 8 shows the Langley and the modified Langley intercepts as a function of wavelength for the airmass interval of the data shown in Fig. 7.

As can be seen from Fig. 8, the modified Langley method improves the retrieval of the intercept in the water vapor bands between 1.3 and 1.5 μm. If the modified Langley approach worked perfectly we would expect that the retrieved intercepts would form a smooth line through the 1.38-μm water band. Several reasons could contribute to the error in the retrieved intercept. The first is that a square root fit may not be the best power law to use for portions of this band. Past work in the 0.94-μm band showed good results from a square root assumption (Volz 1974; Thome et al. 1992), but other work indicates that different exponents may be more appropriate (Pitts et al. 1977; Bruegge et al. 1992). Also, the water vapor absorption in this band is quite high, so it is possible that some of the absorption lines may have saturated in the center of the band. Finally, the modified Langley method assumes that the columnar water vapor is constant throughout the measurement period, and this assumption may not have been valid.

Even so, the results shown in Fig. 8 are good. Further evidence for this is the top portion of Fig. 9 where we have determined the intercept in the water vapor bands by using a curve-fitting routine (dotted line in the figure) of the Langley intercepts. The solid line shows the intercepts obtained from the modified Langley approach. The curve fit was used in the spectral intervals of 1.20–1.30 μm and 1.47–1.75 μm that were chosen because these bands should be unaffected by strong absorption. This curve fit approach assumes the system response is smooth over the entire spectral range for which the fit has been done. The bottom portion of the figure shows the percent difference between the smoothed and the modified Langley intercepts. In most cases, the retrieved intercept is within 5% of the curve fit values. In the interval from 1.15 to 1.3 μm the difference is about 2.5%, and around 1.0% in the 1.5–1.75 μm interval. There is still a 0.05-μm interval (1.33–1.38 μm) where the curve fit and modified Langley intercepts differ by more than 5%. At the strongest water vapor absorption peak, the difference between the intercepts retrieved with the curve fit and the modified Langley methods reaches 40%. The reasons for this large discrepancy are currently being investigated through further data collections and modeling efforts but could be due to the effects mentioned previously.

6. Columnar water vapor retrieval

The total spectral atmospheric transmittance T_{total} can be written as

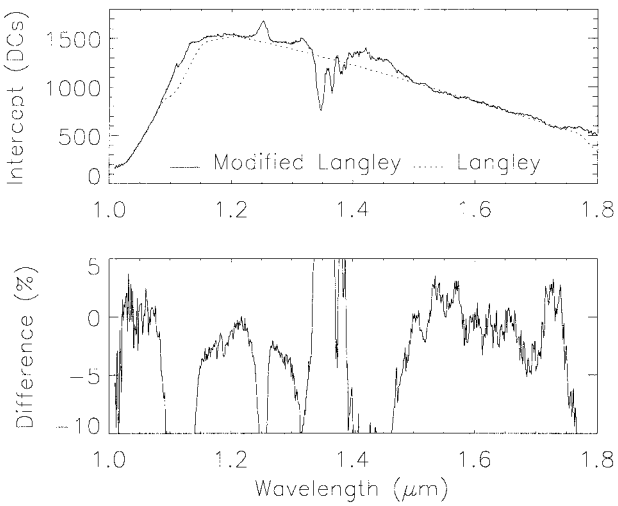

FIG. 9. Intercept from the modified Langley method and smoothed intercept from the Langley method, and percentage difference vs wavelength from the data of the morning of 27 March 1995 for the restricted airmass range from 2 to 6.5.

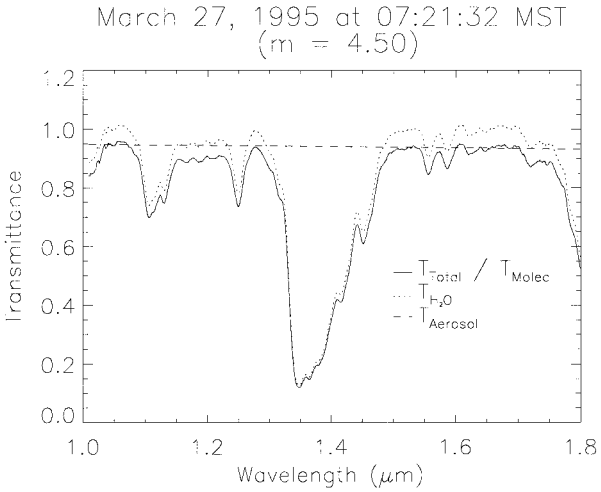

FIG. 10. Total atmospheric transmittance, water vapor transmittance, and aerosol transmittance for an air mass of 4.50 using the data of the morning of 27 March 1995.

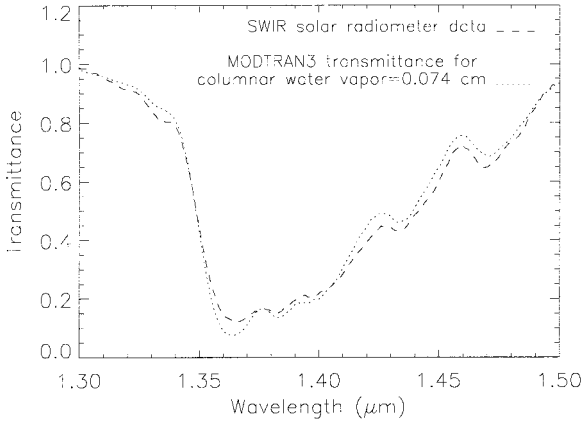

FIG. 11. Transmittance in the 1.38-μm water vapor band derived from SWIR solar radiometer data on the morning of 27 March for a solar zenith of 77.4° compared to MODTRAN3-derived transmittances. The MODTRAN3 data are based on a columnar water vapor amount of 0.074 cm based on VNIR solar radiometer data.

$$T_{\text{total}}(m, \lambda) = \frac{\text{DC}(m, \lambda)}{\text{DC}_0(\lambda)} = T_{\text{molec}}(m, \lambda)T_{\text{aer}}(m, \lambda)T_{\text{abs}}(m, \lambda), \quad (4)$$

where T_{molec}, T_{aer}, and T_{abs} are the transmittances due to molecular scattering, aerosol scattering and absorption, and gaseous absorption, respectively. Figure 10 shows the total atmospheric transmittance for an air mass of 4.50 on the morning of 27 March 1995. The molecular transmittance was determined by assuming Rayleigh scattering and the measured surface pressure. We removed effects of molecular scattering to obtain the solid line in the figure. We assume that aerosol scattering is smooth throughout the spectrum and fit a straight line to data not affected by water vapor—between 1.029 and 1.076 μm and between 1.599 and 1.7 μm. This gives the dashed line in the figure, and correcting for aerosol scattering gives gaseous absorption transmittance shown by the dotted line in Fig. 10.

Figure 11 shows the gaseous transmittance curve specifically for the 1.38-μm water vapor band along with MODTRAN3 results (Berk et al. 1989). The MODTRAN3 results are based on a columnar water vapor amount of 0.074 cm as determined from the 0.94-μm data from the VNIR solar radiometer using the method described by Thome et al. (1992). The input to MODTRAN3 is the *U.S. Standard Atmosphere, 1976* scaled to match the surface temperature and pressure at the Steward Observatory and to give the appropriate columnar water vapor. This corresponds to a slant path water vapor amount of 0.340 cm for the 77.4° solar zenith angle. The SWIR solar radiometer data had to be shifted spectrally by a small amount, 0.015 μm, to have the spectral features in both line up. This shift is required because the transportation of the radiometer most likely affected the alignment of the diffraction grating relative to the detector array. However, because of poor spectral calibration prior to the test, we are not able to determine from where and when the misalignment occurred. The agreement between the two curves is quite good and both the model and experimental data show similar features in the transmittance. This agreement indicates that there is consistency between the two solar radiometers and the modeled MODTRAN3 transmittances.

Figure 12 shows a similar graph of MODTRAN3 transmittances and those from the SWIR solar radiometer. Only here, the columnar water vapor used in MODTRAN3 has been modified to give a better visual fit between the MODTRAN3 output and the measured transmittances. The fit used wavelengths outside of the 1.35–1.40-μm spectral range because a low signal in

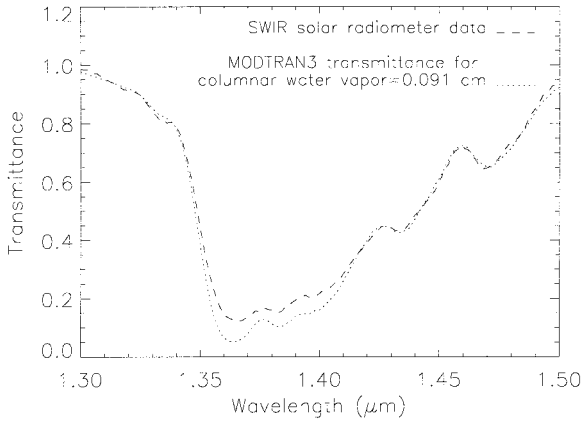

FIG. 12. Transmittance in the 1.38-μm water vapor band derived from SWIR solar radiometer data on the morning of 27 March for a solar zenith of 77.4° compared to MODTRAN3-derived transmittances. The columnar water vapor of 0.091 cm used in MODTRAN3 was selected to give good agreement between the two in the wings of the water band.

this spectral range makes the SWIR radiometer data unreliable. The columnar water vapor showing the best visual fit derived in this fashion is 0.091 cm, as opposed to the 0.074 cm value obtained from the VNIR data. While this type of water vapor retrieval using the hyperspectral SWIR data and MODTRAN3 output may be of limited use because the 1.38-μm water vapor band will saturate at larger columnar water amounts, these results show several important points. First, the calibration of the SWIR radiometer has been done properly and the instrument appears to work well. The good agreement with the MODTRAN3 results show that for these conditions and these wavelengths, MODTRAN3 works very well at predicting atmospheric transmittance. In addition, it still may be possible to use the wings of the 1.38-μm water band for water vapor retrieval at larger columnar water vapor amounts. Further work is needed to fully evaluate these statements and to verify that absorption line saturation and signal-to-noise ratio problems. Finally, a recent update to the MODTRAN code, which includes an improved gaseous absorption database, has been made, and we hope to use it in future studies to estimate better atmospheric transmittances.

7. Aerosol size distribution

The aerosol size distribution is retrieved from spectral optical depths using a method developed by other members of the Remote Sensing Group for use in our vicarious calibration methods (Biggar et al. 1990). This approach assumes a power-law or Junge size distribution and simultaneously retrieves the aerosol size distribution, columnar ozone and optical depths, and aerosol optical depths at wavelengths of interest. When the VNIR solar radiometer is used in this approach, data in the SWIR are extrapolated. By including SWIR measurements, we hope to improve the retrieval of size distribution as well as the prediction of optical depths in the SWIR bands for which we do not have data.

To examine the effects of SWIR data, we use the average optical depths for the morning of 27 March. The average total optical depths for all bands used outside of absorption regions are given in Table 2. We determined the Junge aerosol size distribution from data from only the VNIR solar radiometer (the first nine rows of Table 2) and obtained a Junge parameter of 2.76 and a columnar ozone amount of 0.242 cm atm. The uncertainty of these results based on the work by Biggar et al. (1990) is 0.36 for the Junge parameter and 0.048 cm atm for the columnar ozone. If the same procedure is applied to the full dataset shown in Table 2, the retrieved Junge parameter is 2.61 with an uncertainty of 0.20. The retrieved columnar ozone is still 0.242 cm atm with the same uncertainty. This 6% change in Junge parameter leads to less than a 0.3% change in the radiance at the top of the atmosphere for typical vicarious calibration conditions.

TABLE 2. Total optical depths used to retrieve aerosol size distribution. Data are from both the VNIR and SWIR solar radiometers, as indicated.

Wavelength (μm) and instrument (SWIR or VNIR)	Total optical depth
0.369 (VNIR)	0.3977
0.399 (VNIR)	0.2892
0.440 (VNIR)	0.2059
0.519 (VNIR)	0.1263
0.609 (VNIR)	0.1002
0.669 (VNIR)	0.0635
0.780 (VNIR)	0.0374
0.870 (VNIR)	0.0289
1.027 (VNIR)	0.0206
1.275 (SWIR)	0.0170
1.531 (SWIR)	0.0121
1.661 (SWIR)	0.0167
2.140 (SWIR)	0.0112

This implies that the SWIR data will not significantly change the results of the vicarious calibrations. However, the dataset collected on Mount Lemmon matches a power-law size distribution very well. This means that the addition of the SWIR data should not have much of an effect on the retrieved power-law exponent. There do exist conditions when the power law does not adequately describe the true aerosol size distribution. In these cases, the additional SWIR data will indicate that the power law is not appropriate and the retrieved aerosol size distribution using SWIR and VNIR data could improve the predicted radiances in both the SWIR and VNIR. This will happen in both spectral ranges because the size distribution affects the scattering phase function used in the radiative transfer calculations and the effect of changing the phase function will be larger in the VNIR where the scattering optical depths are larger.

The VNIR-only results can also be used to predict the total optical depths for the four SWIR bands shown. In this case, the predicted VNIR-only optical depths differ from the measured SWIR data shown in Table 2 by 0.0015, -0.0005, 0.0050, and 0.0021, where a negative value indicates the VNIR-derived optical depth is larger. While these differences are large from a percentage standpoint (4%–32%), the effect on predicted radiances at the top of the atmosphere is not significant for the sites that are typically used for vicarious calibration. These sites usually have a reflectance larger than 0.2 and thus the radiative transfer is dominated by the surface reflectance term. This implies that including the SWIR solar radiometer data is not critically important to accurate vicarious calibration. Of course, these effects will be larger for the lower altitude sites, and further datasets will be needed to properly determine the effect.

The results from the above aerosol inversion were also used to assess the effect of the 8° field of view of the SWIR solar radiometer. This large field of view allows more of the forward-scattered light to be measured, leading to larger signals and thus biasing the

results. The retrieved size distribution was used in a radiative transfer code to predict the expected, forward-scattered irradiance. These radiative transfer calculations give the irradiance for a 1° field of view to be 10^{-4} of incident solar irradiance. If this value is assumed to be constant over the entire 8° of the SWIR radiometer's field of view, the result is an increase in the irradiance 0.6%. This value is an overestimate since the forward-scattered radiation falls off by more than a factor of 2 at 4° from the sun. Thus, the forward-scattered radiation should not contribute more than 0.6% to the total signal, and the large field of view for the current configuration should not change the conclusions made in this work.

In general, the results shown in this section give an additional indication that the SWIR solar radiometer data are at least consistent with the VNIR solar radiometer data. Many more measurements are required to show what effect including SWIR optical depths will have on vicarious calibration. Since the primary goal of this work was to evaluate the SWIR solar radiometer, the collection of these additional datasets is not necessary for the current work. Instead, these data collections are planned in future work after the system has been further modified to operate better as a solar radiometer.

8. Conclusions

The results of this work indicate that the SWIR spectroradiometer used here has promise as a solar radiometer. Relative calibration using the Langley method has been shown to be better than 4% in the spectral intervals of 1.15–1.32 μm and 1.47–1.75 μm. Modified Langley calibration extends this to include a portion of the 1.38-μm water vapor absorption band with 5% uncertainty for a large portion of the absorption band. Calibration of the instrument throughout the entire spectral range is accomplished using a curve-fitting approach to the Langley method calibration. Noise in the data for wavelengths longer than 2.0 μm, due to possible diffraction grating housing effects and low signal, currently limits the usefulness of the data at these wavelengths. This noise is decreased by band averaging, thus allowing the data to be useful in determining aerosol size distribution, but should be one of the design requirements for making better SWIR measurements.

The results of the SWIR solar radiometer are also compared to those from a VNIR solar radiometer. The comparisons of optical depth indicate that data from the SWIR solar radiometer are believable. Both instruments show similar trends in average optical depths from day to day and for instantaneous optical depths, but the optical depths from the SWIR solar radiometer exhibit greater variability than the VNIR results around midday. This is most likely due to heating of the diffraction housing of the SWIR system. Columnar water vapor results obtained by the two systems compare to within 0.017 cm (or 0.077 cm in slant path amounts). This shows that the VNIR radiometer, SWIR radiometer, and MODTRAN3 code are consistent with one another. Since the VNIR radiometer has nearly 10 years of use and is fairly well understood, the SWIR system shows good potential for use as a solar radiometer.

The results of the aerosol size distribution retrieval for the one case examined show that the addition of the SWIR data does have a significant effect on the retrieved Junge parameter, which is 6% in this case. The difference between predicted aerosol optical depths based on VNIR-only data and those measured by the SWIR solar radiometer is less than 0.005 for aerosol optical thicknesses on the order 0.015. This again implies the SWIR solar radiometer is operating well since the data are consistent with those of the well-understood VNIR solar radiometer. This result could also be used to infer that the SWIR data are not necessary. However, it should be remembered that these data were collected at a high-altitude site and may not be representative of lower altitudes or more turbid conditions.

Further work is planned to evaluate the improvements that are expected from extending the wavelength range over which atmospheric optical depth measurements are made. Further work is also planned to study methods for improving the SNR for data in the 1.67–2.5-μm spectral region. We plan to improve the field of view of the system to be less than 2° and hope to include an automated tracking mount and data collection. The data collection software will also be modified to allow a larger number of datasets to be collected. Finally, we will attempt to determine the causes of the noisier data for midday data points. With these improvements, the radiometer in this work should provide additional data that should improve the results of our vicarious calibration work.

Acknowledgments. This work was supported by NASA Contract NAS5-31717. The authors wish to thank the Steward Observatory for use of their facilities for this work, and the reviewers' comments for their advice.

REFERENCES

Berk, A., L. S. Bernstein, and D. C. Robertson, 1989: MODTRAN: A moderate resolution model for LOWTRAN 7. GL-TR-89-0122, Geophys. Laboratory, Air Force Systems Command, 38 pp. [Available from Geophysics Laboratory, Air Force Systems Command, Hanscom AFB, MA 01731-5000.]

Biggar, S. F., D. I. Gellman, and P. N. Slater, 1990: Improved evaluation of optical depth components from Langley plot data. *Remote Sens. Environ.,* **32,** 91–101.

——, P. N. Slater, and D. I. Gellman, 1994: Uncertainties in the in-flight calibration of sensors with reference to measured ground sites in the 0.4 to 1.1 μm range. *Remote Sens. Environ.,* **48,** 245–252.

Bruegge, C. J., J. E. Conel, R. O. Green, J. S. Margolis, R. G. Holm, and G. Toon, 1992: Water vapor column abundance retrievals during FIFE. *J. Geophys. Res.,* **97,** 18 759–18 768.

Fujisada, H., 1995: Design and performance of ASTER instrument.

Proc. SPIE Advanced and Next Generation Satellite Symp., Paris, France, SPIE, 16–25.

Gellman, D. I., S. F. Biggar, P. N. Slater, and C. J. Bruegge, 1991: Calibrated intercepts for solar radiometers used in remote sensor calibration. *Proc. SPIE Calibration of Passive Remote Observing Optical and Microwave Instrumentation Symp.*, Orlando, FL, SPIE, 175–181.

Kasten, F., and T. Young, 1989: Revised optical airmass tables and approximation formula. *Appl. Opt.*, **28,** 4735–4738.

Neeck, S. P., C. J. Scolese, and F. Bordi, 1995: EOS-AM1: Project update. *Proc. SPIE Advanced and Next Generation Satellite Symp.*, Paris, France, SPIE, 2–15.

Pitts, D. E., W. E. McAllum, M. Heidt, K. Jeske, and J. T. Lee, 1977: Temporal variations in atmospheric water vapor and aerosol optical depth determined by remote sensing. *J. Appl. Meteor.*, **16,** 1312–1321.

Platnick, S., M. D. King, G. T. Arnold, J. Cooper, L. E. Gumley, and S.-C. Tsay, 1994: Status and calibration of the MODIS airborne simulator for earth remote sensing applications. *Proc. SPIE Platform and Systems EUROPTO Symp.*, Rome, Italy, 91–101.

Slater, P. N., S. F. Biggar, R. G. Holm, R. D. Jackson, Y. Mao, M. S. Moran, J. M. Palmer, and B. Yuan, 1987: Reflectance- and radiance-based methods for the in-flight absolute calibration of multispectral sensors. *Remote Sens. Environ.*, **22,** 11–37.

Smith, M. W., 1992: Design and initial performance evaluation of a portable shortwave infrared spectroradiometer. *Proc. SPIE Infrared Technology XVIII Symp.*, San Diego, CA, SPIE, 118–134.

——, 1994: Calibration and performance evaluation of a portable shortwave infrared (1.05 to 2.45 μm) spectrometer. *Opt. Eng.*, **33,** 5811–5819.

Thome, K. J., B. M. Herman, and J. A. Reagan, 1992: Determination of precipitable water from solar transmission. *J. Appl. Meteor.*, **31,** 157–165.

——, M. W. Smith, J. M. Palmer, and J. A. Reagan, 1994: Three-channel solar radiometer for the determination of atmospheric columnar water vapor. *Appl. Opt.*, **33,** 5811–5819.

Volz, F. E., 1974: Economical multispectral sun photometer for measurements of aerosol extinction from 0.44 microns to 1.6 microns and precipitable water. *Appl. Opt.*, **13,** 1732–1733.